COMMUNICATIONS: SIF Congress 2010

X-ray tomographic techniques for the study of cultural heritages

T. SCHILLACI(*)

*Dipartimento di Fisica e Tecnologie Relative, Università di Palermo - Viale delle Scienze Ed. 18
90128 Palermo, Italy*

Summary. — In recent years, X-ray Computed Tomography (CT) has become an
important tool for investigating all kinds of materials. Due to its non-destructive
nature, it is especially suitable to investigate samples that may not be altered or
damaged during the course of the investigation. CT has been recently introduced
in the field of Cultural Heritage diagnostics, where it can be used for the investi-
gation of different works of art, as it preserves the integrity of the object and gives
morphological and physical information on its inner structure. This paper describes
a methodological approach on the use of the X-ray CT technique to study items
belonging to cultural heritage with the aim to obtain information related to their
preservation state and therefore, to plan an adequate conservation and restoration
procedure. Significant examples of applications are the study of porosity and pore
size distribution and their connectivity for different porous materials and the study
of kinetics of capillary fluid absorption in sedimentary rocks. Other applications are
relevant to the possibility to investigate in a non-destructive way the presence of
defects or fractures inside an object and, not last in order of importance, the possi-
bility to study different typologies of woods or waterlogged woods, the presence of
an eventual biodegradation state and the possibility to perform a dendrochronology.
In this paper, the results of some case studies, obtained through the integrated use
of CT systems with different resolutions, are reported. Other expected future devel-
opments will be addressed to the integration of CT data with results of compatible
non-destructive techniques.

PACS 07.60.-j – Optical instruments and equipment.
PACS 42.79.Pw – Imaging detectors and sensors.

1. – Introduction

X-ray Computed Tomography (CT) is a non-destructive technique that uses X-ray
transmission images of a sample and allows to reproduce sections of its structure and the
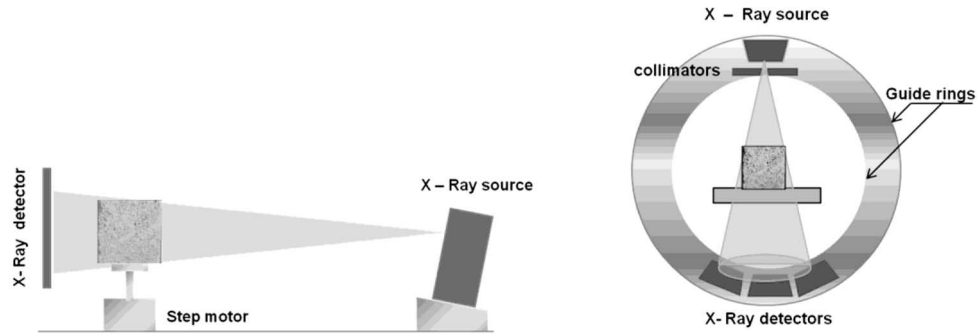

(*) E-mail: tschillaci@unipa.it

Fig. 1. – A schematic view of two tomographic devices operating with two X-ray beam geometric configurations. On the left the *cone beam* geometry and, on the right, the *fan beam* geometry.

3D visualization of the internal part, determined by variations in density and atomic composition [1, 2]. CT images record differences in the degree of attenuation of the X-rays, which is material land energy-dependent. The interactions that are responsible for this attenuation are mainly Compton scattering and photoelectric absorption. The contribution of the photoelectric effect depends on the effective atomic number and is especially important at low energies. At high energies, the Compton effect predominates and attenuation is mainly determined by density [1]. X-ray CT was developed as a medical imaging technique in the early 1970s [3]. The possibility of its use in geology and engineering was soon recognised, resulting in large numbers of publications from the early 1980s onwards. Early applications include studies in the fields of soil science [4,5], meteoritics [6], petroleum geology [7,8], palaeontology [9], geotechnics [10] and sedimentology [11]. CT has been recently introduced in the field of Cultural Heritage diagnostics [12-20], where it can be used for the investigation of different works of art, as it preserves the integrity of the object and gives morphological and physical information on its inner structure [19]. The knowledge of these features is very useful for determining adequate conservation and restoration procedures. Information can be retrieved as 2D cross-section images or 3D full-volume images allowing the inspection and the classification of the object; moreover, by processing tomographic data, a 3D numerical model of the sample can be obtained for virtual-reality applications or digital-archives storage [18, 19]. A tomographic device is essentially composed by an X-ray source and a detector and the object to analyse is put between them. The X-ray beam can be collimated and this is commonly known as *fan beam* geometry; otherwise it's known as *cone beam* geometry. The *fan beam* geometry is the common one, as in the widely used medical CT devices. Most common X-ray tubes produce a cone of radiation with a certain angle, usually 30 degree of aperture, so that they need a slit collimator to have a *fan beam*. A further step in computed tomography analysis is the reconstruction and the visualisation of a three-dimensional volume, basically composed of the attachment of many tomographic slices [14]. This approach is right for most common *fan beam* geometry systems, but there exists a special algorithm called *Feldkamp algorithm* [21] that allows to use the *cone beam* geometry as well as to obtain a reconstructed three-dimensional volume from a set of two-dimensional projections, *i.e.* a set of radiographies of the sample collected at every angle around the objects. A schematic view of the two principal types of tomographic devices that use the *fan bean* and the *cone beam* geometries are shown in fig. 1. In the figure, on the left, a schematic

view of a CT that uses the *cone beam* geometry is shown, and in this case the X-ray source and the planar detector are fixed with the sample that rotates with respect to a vertical axis. On the right of the same figure, a schematic view of a CT system that uses a *fan beam* geometry is shown, and in this case the X-ray source and the detector rotate in synchronous modality around the object that translates with respect to the perpendicular direction of the rotation plane.

The development of X-ray sources and detectors more and more efficient in terms of high intensity and spatial and energetic resolution, respectively, jointly with the improved elaboration data systems, allow to obtain images with micro- and also nano-metric resolutions [12, 15-19]. The possibility to have images with a high spatial resolution with faster acquisition times allows to study dynamic physical phenomena as the capillary flow absorption in porous materials [12]. The main set-up parameters that influence the image qualities are the voltage and the anodic current, the acquisition time, the FOV (Field of View), the image resolution and the acquisition and elaboration filters used. In this paper, the results of some case studies are reported, obtained through the combined use of two CT systems with different resolutions. The CT image acquisitions were performed in collaboration with the Department of Biopathology and Medical and Forensic Biotechnologies (DiBiMeF), the Radiological Science Division of the University of Palermo and the Institute for Agricultural and Forest Systems of the Mediterranean area (ISAFOM) of the Italian National Research Council.

Materials and methods

The CT image acquisitions were performed with a medical device Philips Brilliance 64 (Philips, Eindhoven, The Netherlands) operating at the Radiological Science Division of the Department of Biopathology and Medical and Forensic Biotechnologies (DiBiMeF) of the University of Palermo and with a micro-tomographic system Skyscan 1172 (Skyscan, Kontich, Belgium) operating at the Institute for Agricultural and Forest Systems of the Mediterranean area (ISAFOM) of the Italian National Research Council.

With reference to the medical CT system, the instrumental set-up values were selected in order to obtain the maximum spatial resolution with a low Signal-to-Noise Ratio (SNR). The instrument operated with a voltage of 120–140 kV, an anodic current of 250–600 mA, a slice thickness of 670 μm and a resolution of 50 μm. The micro CT set-up values were settled with an operating anodic tension of 60–110 kV, a current of 100–200 mA and a maximum resolution of 1.3 μm. Different kinds of materials, lapideous, wooden and bonny, were analyzed in order to demonstrate the investigative potentiality of these techniques for the study of cultural heritage. In fig. 2 we report the pictures of the sedimentary rock samples, litho-type materials among those used for the building of the historic monuments of the Greek and Baroque period present in Sicily and coming from quarries located close to the archaeological sites.

In order to study the kinetics of the capillary water absorption in the sedimentary rocks samples, aimed to understand the degradation processes in monuments due to this phenomenon and to attend a suitable conservation procedure, CT image acquisitions were performed with the medical CT Philips Brilliance 64. The samples were cubic shaped (50 mm $\times$ 50 mm $\times$ 50 mm) and images in dry conditions and at different times from the water contact were acquired with a time sequence of 120, 240, 360, 900, 1320, 2100, 3300 and 5100 s, respectively. Previously gravimetric measurements were performed on the same samples as always according to the standard UNI 10825 procedure [22]. The main idea was to monitor the CT values registered for each voxel as soon as the water fills the

Fig. 2. – A picture of the sedimentary rocks coming from the Sicilian quarries. From the left Agrigento, Cusa and Noto samples.

pores in the material pushed by the capillary forces. The CT number is defined by the following equation:

$$\text{(1)} \qquad\qquad \text{CT} = \frac{\mu_{\text{voxel}} - \mu_{\text{water}}}{\mu_{\text{water}} - \mu_{\text{air}}} \cdot 1000,$$

where μ_{voxel}, μ_{water} and μ_{air} are the linear absorption coefficients for X radiation in the voxel, for water and for air, respectively. According to the CT number definition, if the voxel is filled by air, the CT value is -1000, for water is zero. In the case of bone the CT number is in the range 900–1000. For the sedimentary rock samples, where calcium is the main element, typical values are in the range 1300–1400 due to the higher density in comparison with bones. The voxel dimensions are $50\,\mu\text{m} \times 50\,\mu\text{m} \times 670\,\mu\text{m}$. For each slice we obtain a matrix of CT values $A(\text{CT}_{i,j,})$ where the suffix i and j are related to the row and column numbers and each matrix is updated at the different times (t_k) from the water contact obtaining a scalar values matrix $A(\text{CT}_{i,j},\ t_k)$ for each sample. The CT scalar value matrix obtained for each slice, has been elaborated by the MATLAB software. The micro CT images were acquired on small samples of the order of 5 mm in diameter and 10 mm height drilled from the same sedimentary rock samples analysed by CT technique.

Bony human finds recovered in an archaeological excavation in the northern part of Sicily, were analyzed through the medical CT and the micro CT systems. In fig. 3 we report the images of some samples, a thighbone shown on the left, a vertebra and a rib shown on the left of the same figure.
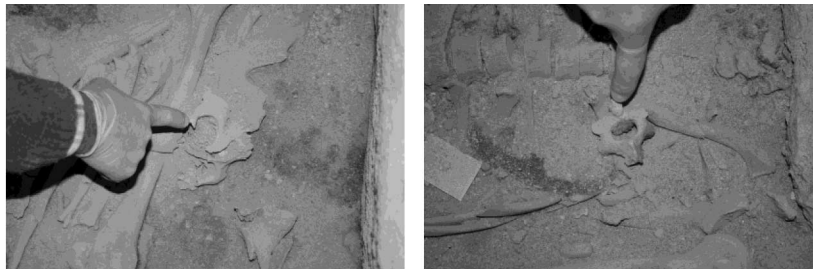

Fig. 3. – A picture of the thighbone sample on the left and, on the right, the vertebra and the rib samples.
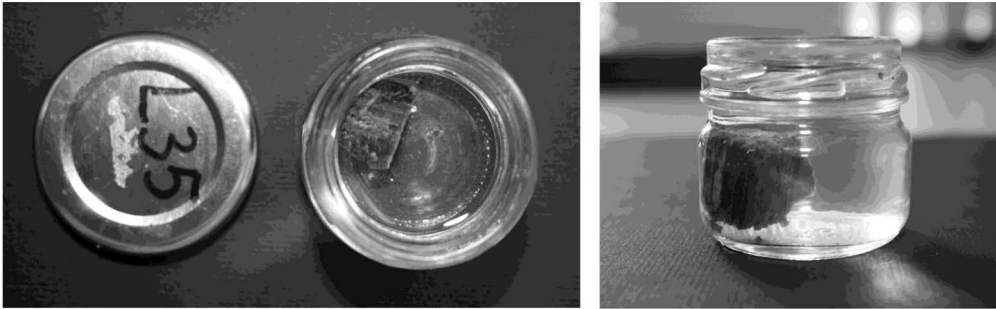
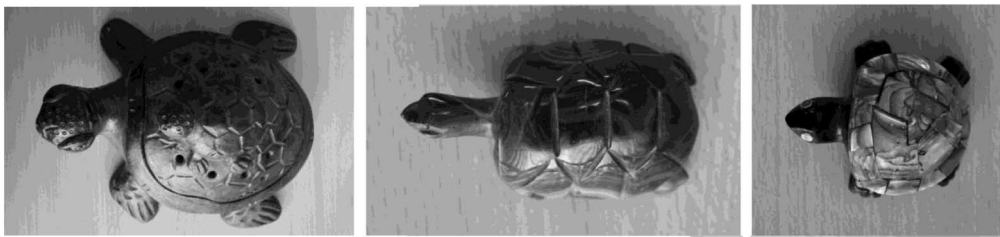Fig. 4. – Pictures of a waterlogged wood sample.

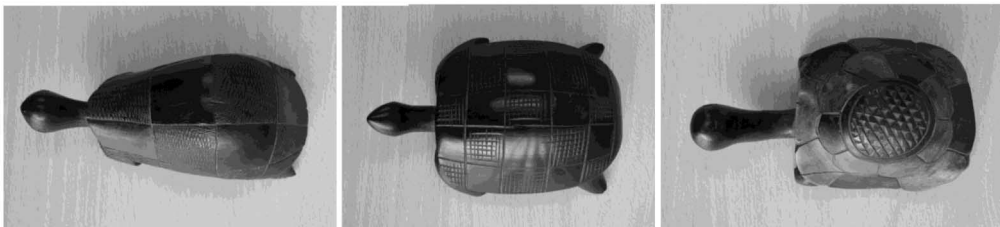Fig. 5. – Pictures of three turtles made with different materials.

Fig. 6. – Pictures of three turtles made of different kinds of wood.

Micro X-Ray CT image acquisitions were performed also on waterlogged wood samples withdrawn from a roman ship, recently found in the Sicilian coast near the city of Trapani (locality Marausa). A picture of one sample is shown in fig. 4. Moreover, in order to test the applicability of the X-Ray CT imaging techniques to objects of different materials, turtles made with different materials were analyzed by the medical CT instrument. In fig. 5, from the left to the right, three turtles made in ceramics, marble and obsidian, respectively, are shown, the latter coated by a pearly layer. Moreover, in fig. 6 three wooden turtles made with different kinds of wood are shown.

2. – Results and discussions

In fig. 7 the pore size distribution of the sedimentary rock samples, obtained by the analysis of the micro CT, is reported. It is related to the volumetric distribution of the connected pore spaces. The results show a narrow pore size distribution centred
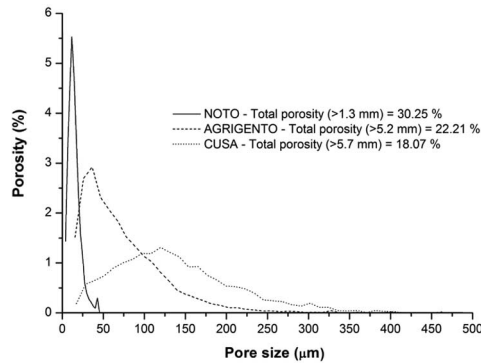
Fig. 7. – Pore sizing distribution for the sedimentary rock samples.

around 25 μm for the *Noto* sample that exhibits also a bimodal distribution; moreover, a spread pore size distribution centred at about 50 μm for the *Agrigento* sample and a more spread pore size distribution centred at about 125 μm for the *Cusa* sample can be observed. Obviously only pore spaces larger than the image resolution can be detected, therefore the above values of total porosity do not include contribution of possible pores smaller than the resolution. The pore size distribution has been calculated using the "opening" algorithm [23-25] which is an operator of mathematical morphology. Such procedure allows to classify the pore space according to the pore walls distance. In other words, in the graphs reported in fig. 7, at each pore size there corresponds the volume of the pore space having that distance from the walls. The area subtended for each pore size distribution curve represents the total porosity of each sample. In fig. 8 the cumulated pore size distribution, obtained through the integral calculation of the data reported in fig. 7, is reported. The *Noto* sample showed a total porosity of 30.25%. The *Agrigento* and *Cusa* samples showed a total porosity of 22.21% and 18.07%, respectively.

A zoom of the pore size bimodal distribution for the *Noto* sample is shown in fig. 9. The three-dimensional connectivity analysis is reported in fig. 10. It is based on the percolation curves. These latter are drawn performing a successive elimination of the pores of increasing size on the 3D images and each time only the porosity connected
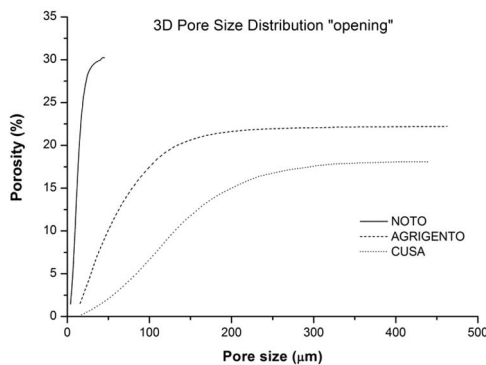

Fig. 8. – Pore size distribution cumulated for the sedimentary rock samples.
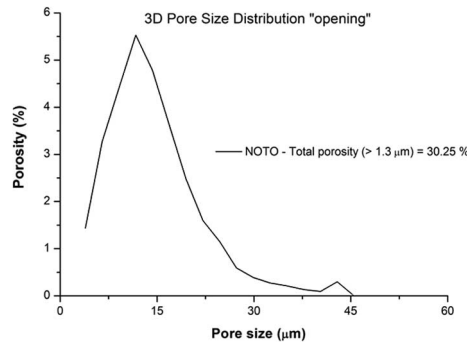
Fig. 9. – Pore sizing distribution for the *Noto* sample.

between couples of the opposite faces of the samples is considered. The curves in fig. 10 show that the *Noto* sample is initially the most connected while, after the elimination of the smallest pores, the curves of *Cusa* and *Agrigento* show higher values. The pore sizes where the connected porosity becomes zero are called percolation thresholds. These values are $14\,\mu$m and $57\,\mu$m for *Noto* and *Agrigento*, respectively, while for *Cusa* the percolation threshold ranges between $86\,\mu$m and $108\,\mu$m depending from the direction of the analysis. Such results mean that *Noto* has the more completely connected porosity, while a given level of connectivity is guaranteed by larger pores for the *Cusa* and *Agrigento* samples. Moreover, *Noto* is perfectly isotropic while *Cusa*, in particular, exhibits a certain degree of anisotropy of the pore network.

In fig. 11 we report the CT scalar value matrices $A(\mathrm{CT}_{i,j},\,t_k)$ registered for the *Noto* sample and relative to a single slice and at different acquisition times. The first image, upper left, is related to the dry condition, the others, from left to right and downwards are related to the different times from the contact with water. The data are reported as images in false colours. The images show the variations of the CT number registered for each voxel as soon as the water fills the porous space pushed by capillary forces. The dashed gray line in the images shows schematically the moving of the wetting water front that in this case is rather flat, as a piston-like movement, according to the theoretical
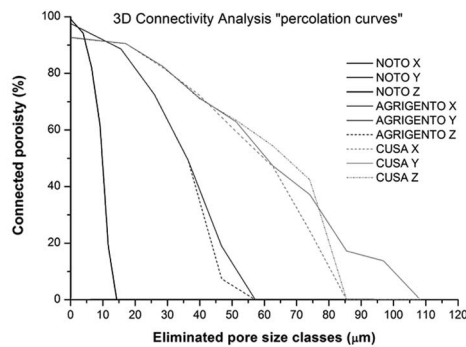

Fig. 10. – 3D pore sizing distribution for the *Noto* sample.
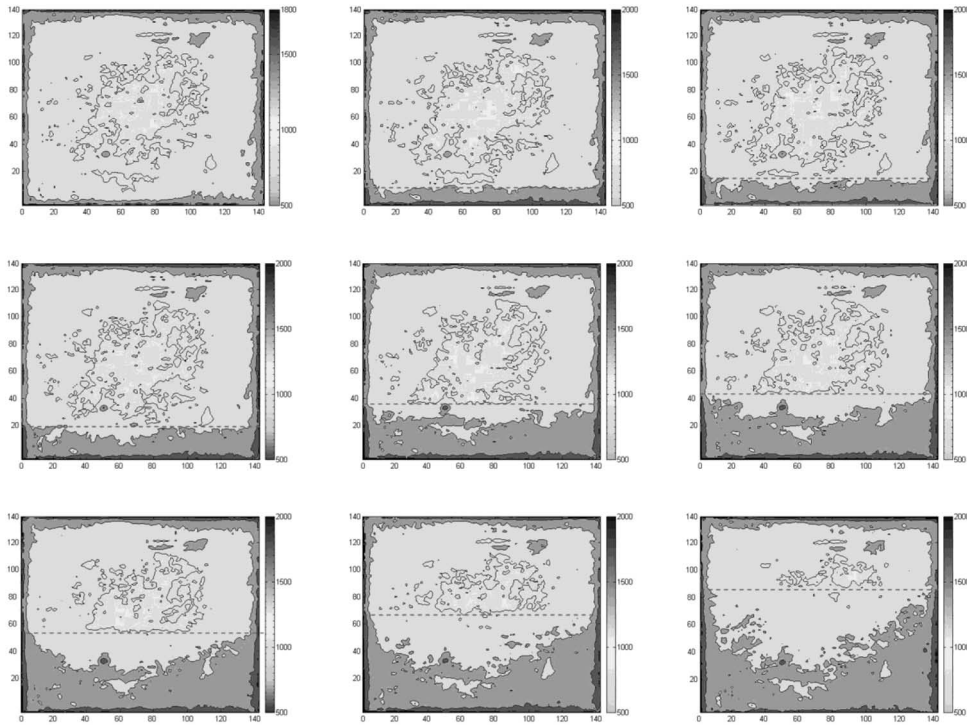
Fig. 11. – Water imbibition in the sedimentary rock (*Noto* sample) shown as variation of the CT number at different times from the contact with water. The first image (upper left) is related to the dry condition, the other ones are acquired at different times.

Handy model [26]. The colour bar on the right of each image shows the range of the CT values. At different times from the contact with water the CT number registered for each voxel is increasing from the bottom up to the upper part of the sample due to the water filling of the pore spaces. The lowest CT values of the central part of the slice are related to the lowest dose radiation value. In fig. 12 the scalar values matrix $A(\mathrm{H}_{i,j}, t_k)$ registered for the *Agrigento* sample are reported.

In the case of the *Agrigento* sample, due to the heterogeneity of the material and at the different inclusions of small marine shells and pebbles, the kinetic of water absorption is governed by stochastic percolation models [27]. In this case the water front does not present a regular shape.

Considering a square Region of Interest (ROI), large as the sample dimensions in our case, a mean value of the CT scalar values related to a fixed slice for each sample and at different times from the contact with water was calculated. In fig. 13, on the left, we report the water absorption curves obtained by evaluating the CT number values at different times from water imbibition and shown as CT number *versus* the square root of time. The data were evaluated as the mean value of the CT values relative to four different slices of each sample. In the same figure, on the right, we report the water absorption curves obtained by the gravimetric method and shown as the water absorption coefficient Qi expressed as quantity of water per surface area *versus* the square root of
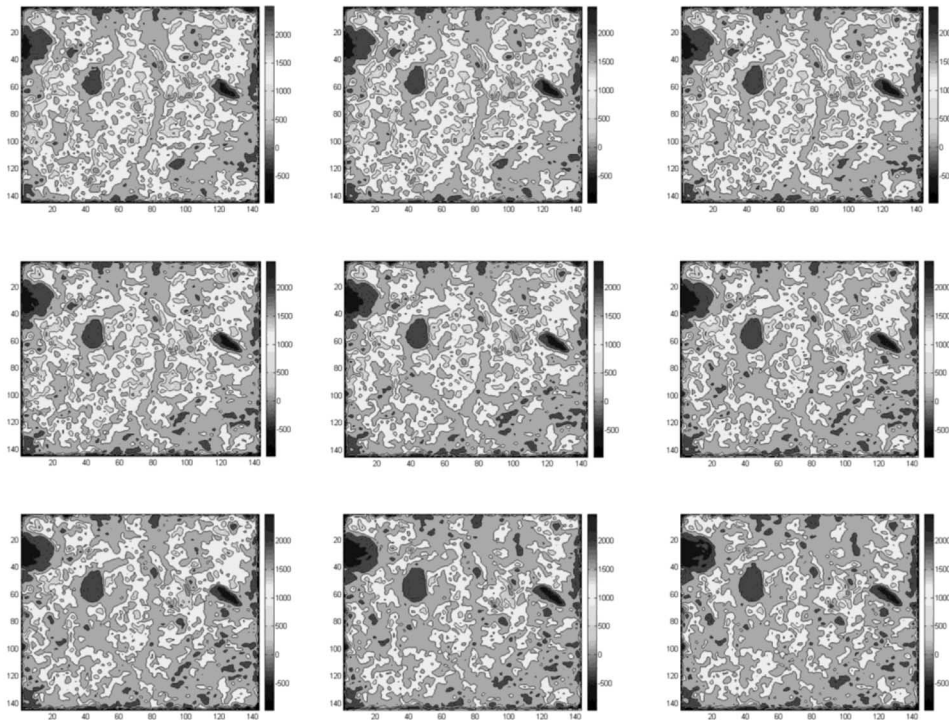
Fig. 12. – Water imbibition in the sedimentary rock (*Agrigento* sample) shown as variation of the CT number at different times from the contact with water. The first image (upper left) is related to the dry condition, the other ones are acquired at different times.

time. In this case the data are related to four samples of each sedimentary rock. The plots reported on the left of fig. 13, well fitted by a straight line, are in good agreement with the data obtained through the gravimetric method. The *Cusa* sample reaches the saturation condition before the other ones and show a higher value of the water absorption curve gradient.

The information provided through the use of the CT techniques in terms of porous features and kinetics of capillary water absorption of materials used in cultural heritages are fundamental to the purpose of a perfect planning of a conservative or restorative intervention.

The same image analysis procedures applied on the pore networks of the sedimentary rocks has been performed on the trabecular network of the bone samples shown in fig. 3. A trabecula represents the inner part of the bone samples which characterizes the mechanical behavior of the bones. Therefore, in this case, we have studied the solid phase of the sample. In fig. 14, we report, on the left, a micro CT slice of the rib sample and, on the right, its volumetric reconstruction. Figure 15, on the left, shows the monomodal pore size distribution around the value of $180 \, \mu$m and the percolation threshold, shown in fig. 15, on the right, at the same value. Such results, together with the overall isotropy of the connectivity, indicate the regularity and homogeneity of the trabecular network of the sample which is typical of a healthy tissue. This is a particularly important result given
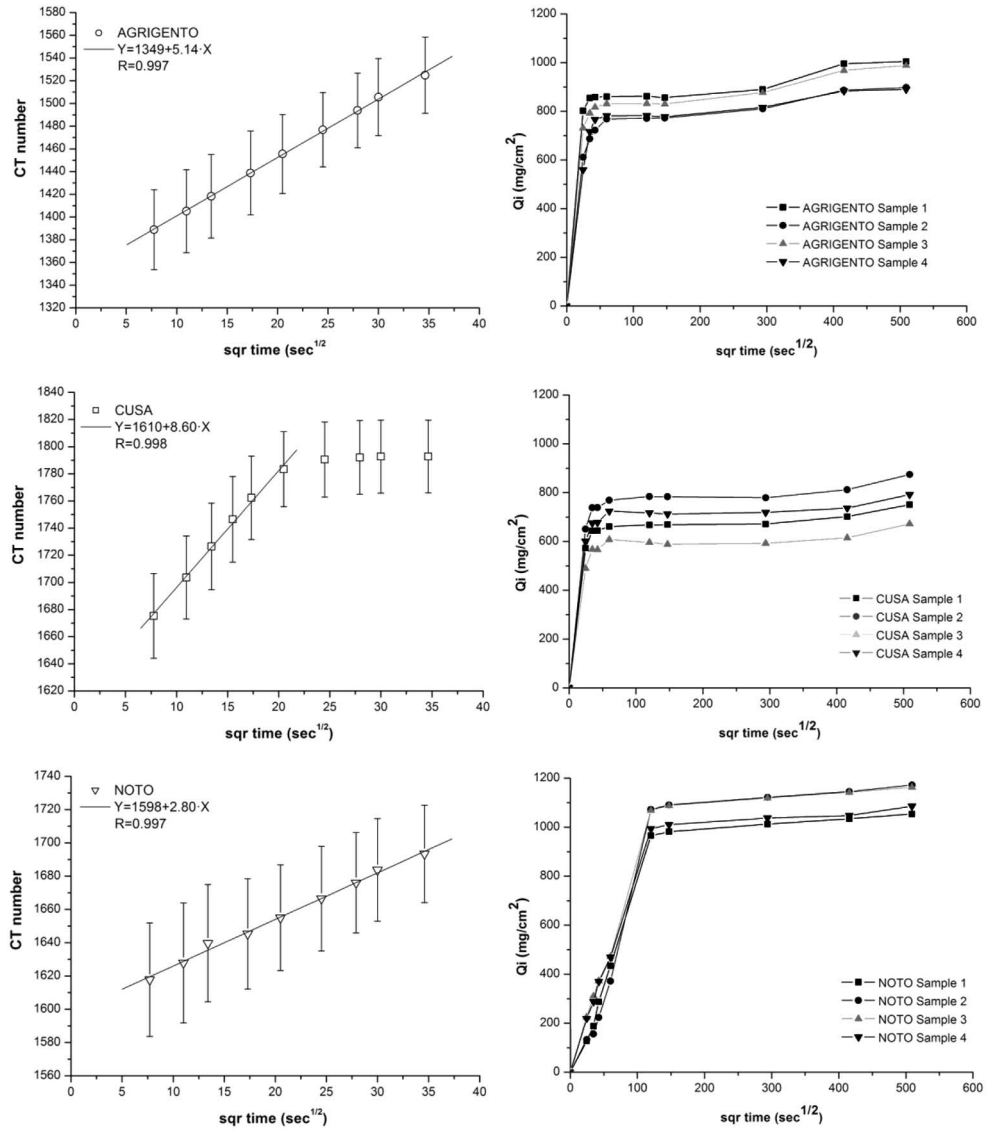
Fig. 13. – Capillary water absorption. On the left, the CT values as a function of the square root of the time are reported. On the right, the water absorption coefficient Qi as a function of the square root of time.

that it is possible, by the comparison with the values of healthy people, to understand whether the person could eventually be affected from osteoporosis disease.

In fig. 16, on the left, a CT slice of the head of thighbone sample and, on the right, a micro CT slice of a vertebra are shown. The images shown, at the same dimensions, are related to samples of different dimensions: the head of a thighbone, about 8 cm large, and a small part of a vertebra of about 2.5 cm. The images show the different spatial resolution.
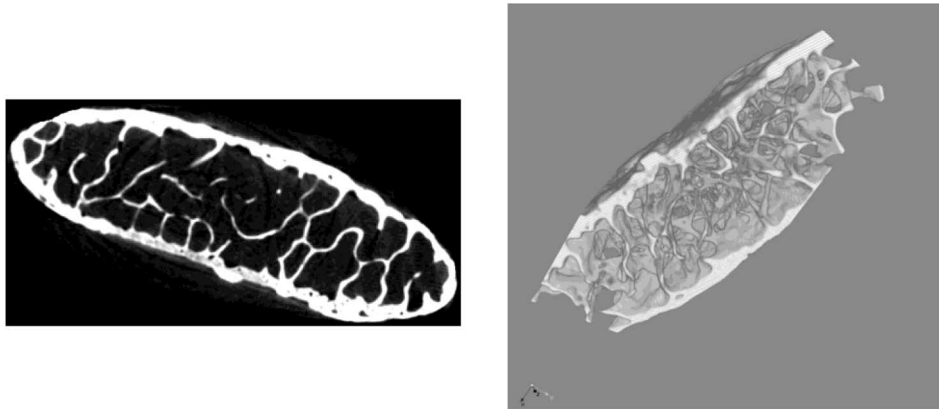
Fig. 14. – A micro CT slice of a rib on the left. On the right the volumetric reconstruction.

In fig. 17, on the left, the micro CT slice of the waterlogged sample and, on the right, the volumetric reconstruction are shown. The images show the characteristic rings of the wood and, moreover, the presence of resinous ducts. From the analysis of these images it is possible to define the kind of wood which, in this case, is a conifer and probably a fir, a wood enough used to build some parts of ships. Also in this case, the micro CT techniques is a very useful non-destructive technique to study the structural wood integrity and, moreover, the wood type.

Moreover, due to the spatial resolution it is possible to study also any possible biodegradation processes due to bacterial colonies.

In fig. 18, on the left, a CT slice of an empty turtle made in ceramic is reported. One can see two turtles inside it: on the left side, one made of obsidian with a top pearly surface, the other one, on the right side, made of serpentine marble. The porous structure of the ceramics is well visible with respect to the other two turtles that show a more compact structure. From this slice, the pearly surface of the turtle on the left inside the turtle in ceramic is also visible, while the serpentine marble turtle shows some
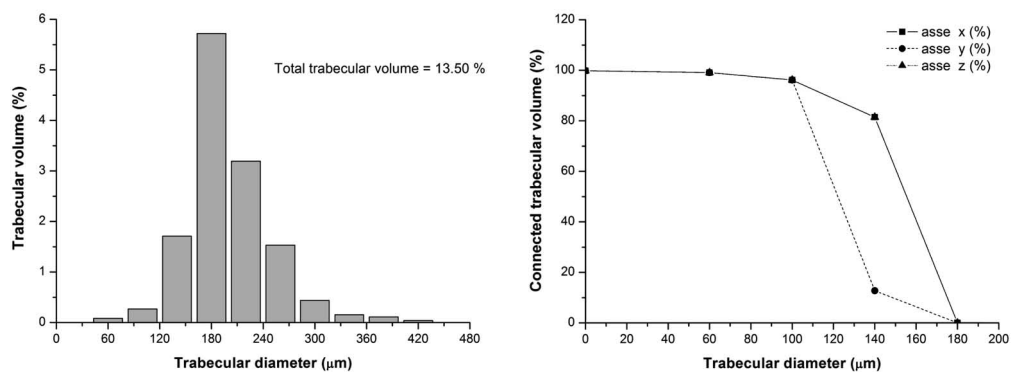

Fig. 15. – The trabecular diameter size distribution of the rib sample on the left. On the right, the trabecular connectivity.
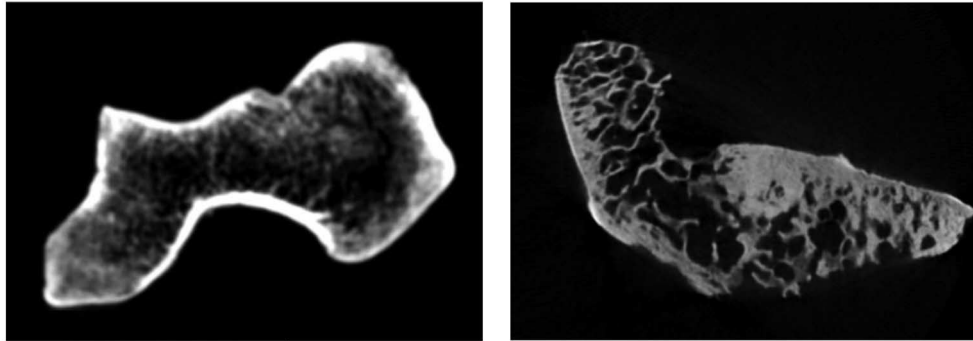
Fig. 16. – On the left, a CT slice of the thighbone sample and, on the right, a micro CT slice of the vertebra sample.

artefact due to the higher-density material. On the right of fig. 18, one can see a three-dimensional sketch of the inside of the bigger turtle made in ceramic with, evidenced, the two turtles inside it. The potentiality offered by the software elaboration of the data that allowing to undertake a virtual inspection of the inner parts of an object is very useful in the field of cultural heritages to study the inner structures in a non-destructive way. This feature is very useful to look inside an object to explore the presence of other objects or internal defects, fractures or the presence of metallic or wooden inserts.

In fig. 19 we report, on the left, a CT slice of a wooden turtle with, evidenced, the presence of an internal defect reported in the right upper part of the image and a fracture shown on the left. The image on the right shows a volumetric CT image reconstruction of the same wooden turtle, with, evidenced, three metallic inserts connected with the core part of the building material at higher density with respect to the other parts.

The CT technique is a very powerful non-destructive technique that allows to differentiate wooden objects made with different materials. In fig. 20 we show, on the left,
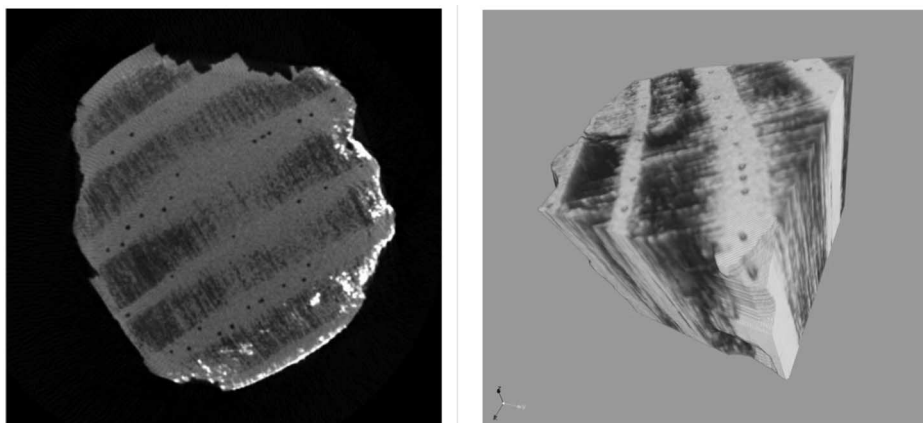

Fig. 17. – A micro CT slice of a wood sample on the left. On the right its volumetric reconstruction.
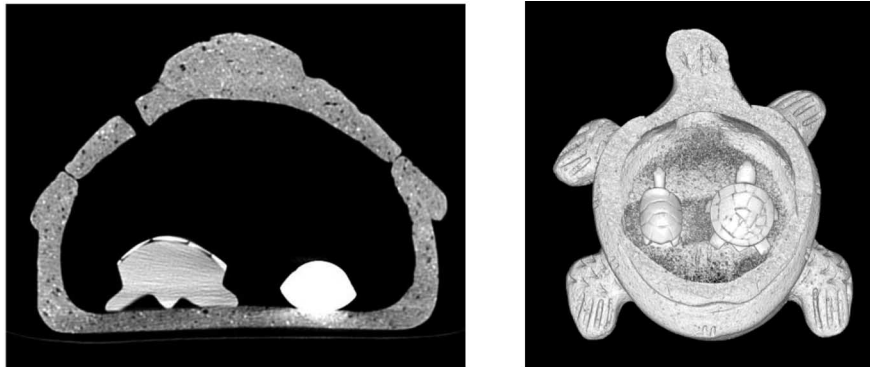
Fig. 18. – A CT slice of a ceramic turtle on the left. On the right, its volumetric reconstruction.

the CT slices of three turtles made with different wood typologies and, on the right, the volumetric CT image reconstruction.

Analyzing the structure of the wood rings it is possible to understand the different typology of the wood used and, moreover, it is possible also to perform a dendrochronology. These are very interesting results for the study of wooden artworks.

3. – Conclusions

The results show the remarkable potentiality of the non-destructive X-ray CT imaging technique for the study of cultural heritages. The images were obtained with different spatial resolution through the integrated use of two tomographic instruments. The instrumental set-up values are related to the different kinds of material to be analysed and of the expected spatial resolution. The medical CT instruments allow to perform the study of dynamic phenomena as the capillary water absorption in porous materials thanks to the fast image acquisition speed. For small samples the micro tomographic technique allows the study of the micro-sized features as the pore size distribution of porous material and the densitometry study of bonny finds. The possibility to differentiate wooden objects made with different woods and to perform a dendrochronology is a very interesting result in the field of archaeometry. Further research projects are oriented
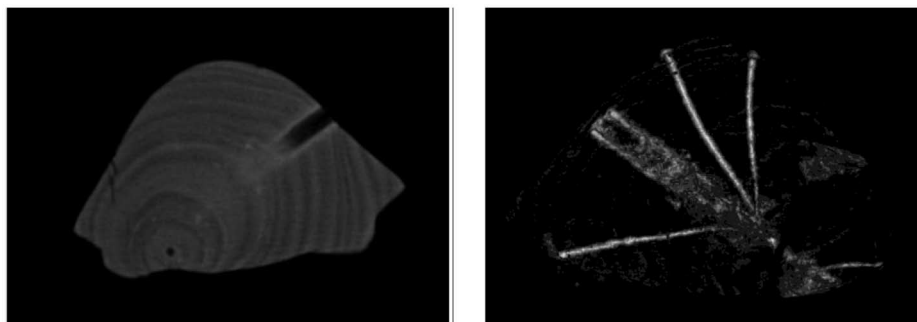

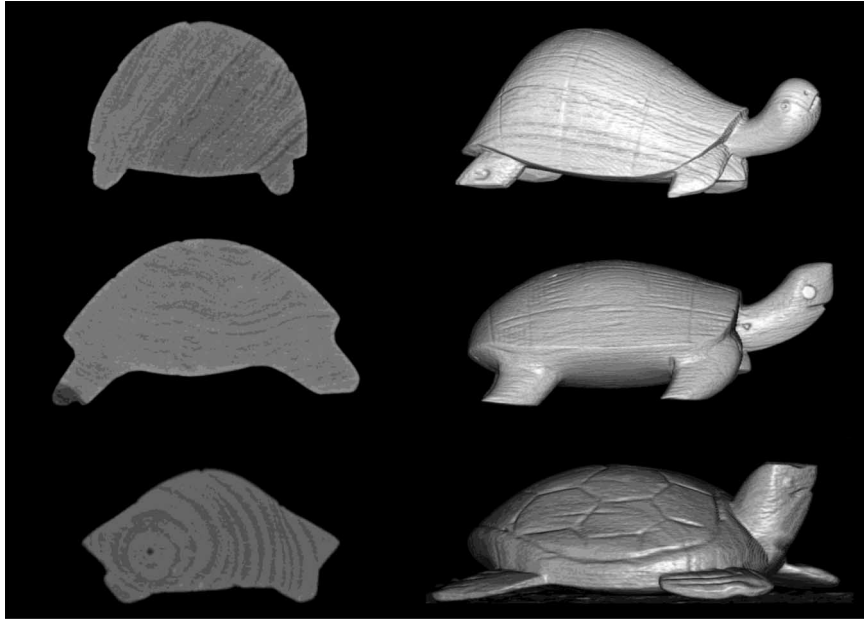Fig. 19. – A CT slice of a wooden turtle on the left. On the right, its volumetric reconstruction.

Fig. 20. – CT slices of the wooden turtles on the left. On the right, their volumetric reconstruction.

to the design and realization of a portable tomographic instrument addressed to the the integration of CT data with results of compatible non-destructive techniques.

* * *

REFERENCES

[1] Mees F., Swennen R., Van Geet M. and Jacobs P., in *Application of X-Ray Computed Tomography in the Geosciences*, edited by Mees F., Swennen R., Van Geet M. and Jacobs P., Vol. **215** (Geological Society, London) 2003, pp. 1–6.
[2] Zitha P. L. J., Nguyen Q. P. and Currie P. K., *Trans. Porous Media*, **64** (2006) 301.
[3] Hounsfield G. N., *British J. Radiol.*, **46** (1973) 1023.
[4] Petrovic A. M. and Siebert J. E. and Rieke P. E., *Soil Sci. Soc. Am. J.*, **46** (1982) 445.
[5] Mele G., Basile A., Leone A. P., Moreau E., Terribile F. and Velde B., in *Modelling of Transport Processes in Soils*, edited by Feyen J. and Wiyo K. (IUSS, Leuven) 1999, pp. 103–117.
[6] Arnold J. R., Testa J. P. J., Friedman P. J. and Kambic G. X., *Science*, **219** (1982) 383.

[7]   VINEGAR H. J., *Petr. Technol.*, **38** (1986) 257.
[8]   SANTOS L. O. E., PHILIPPI P. C., DAMIANI M. C. and FERNANDES C. P., *J. Petrol. Sci. Eng.*, **35** (2002) 109.
[9]   HAUBITZ B., PROKOP M., DOHRING W., STROM J. H. and WELLNHOFER P., *Paleobiology*, **14** (1988) 206.
[10] RAYNAUD S., FABRE D., MAZEROLLE F., GERAUD Y. and LATIÈR H. J., *Tectonophysics*, **159** (1989) 149.
[11] KENTER J. A. M., *Mar. Geotechnol.*, **8** (1989) 201.
[12] ALBERGHINA M. F., BARRACO R., BRAI M., LO CASTO A., MAZZOCCHIO A. and SCHILLACI T., in *Proceedings of Optics for Arts, Architecture, and Archaeology II*, edited by PEZZATI L. and SALIMBENI R. (SPIE, Munich) 2009, p. 73910Y-1.
[13] APPLBAUM N. and APPLBAUM Y. H., in *X-Rays for Archaeology*, edited by UDA M., DEMORTIER G. and NAKAY I. (Springer, Berlin) 2005, pp. 231–245.
[14] BETTUZZI M., BRANCACCIO R., CASALI F., CORNACCHIA S., GIORDANO M., MORIGI M. P., PASINI A. and ROMANI D., in *Proceedings of the International School of Physics "Enrico Fermi"*, Course CLIV, edited by MARTINI M., MILAZZO M. and PIACENTINI M. (IOS Press, Amsterdam; SIF, Bologna) 2003, p. 461.
[15] BUGANI S., CAMAITI M., MORSELLI L., VAN DE CASTEELE E. and JANSSENS K., *X-Ray Spectrom.*, **36** (2007) 316.
[16] BUGANI S., CAMAITI M. and MORSELLI L., *Anal. Bioanal. Chem.*, **391** (2008) 134.
[17] ROSSI M., CASALI F., CHIRCO P., MORIGI M. P., NAVA E., QUERZOLA E. and ZANARINI M., *IEEE Trans. Nucl. Sci.*, **46** (1999) 897.
[18] MORIGI M. P., CASALI F., BETTUZZI M., BIANCONI D., BRANCACCIO R., CORNACCHIA S., PASINI A., ROSSI A., ALDROVANDI A. and CAUZZI D., *Nucl. Instrum. Methods Phys. Res. A*, **580** (2007) 735.
[19] MORIGI M. P., CASALI F., BETTUZZI M., BRANCACCIO R. and D'ERRICO V., *Appl. Phys. A*, **100** (2010) 653.
[20] SCHILLACI T., BRAI M., CIMINO A., LO CASTO A. and SORRENTINO F., *Cons. Sci. Cult. Herit.*, **8** (2008) 91.
[21] FELDKAMP L. A., DAVIS L. C. and KRESS J. W., *J. Opt. Soc. Am. A*, **1** (1984) 612.
[22] UNI 10859, *Norma Italiana Beni Culturali, Materiali lapidei naturali e artificiali: determinazione dell'assorbimento d'acqua per capillarità* (2000).
[23] SERRA J., in *Image Analysis and Mathematical Morphology*, Vol. **1** (Academic Press, London) 1982, p. 661.
[24] HORGAN G. W., *Eur. J. Soil Sci.*, **49** (1998) 16.
[25] SOILLE P., in *Morphological Image Analysis—Principles and Applications* (Springer, Berlin) 2003, p. 391.
[26] HANDY L. L., *Petr. Trans.*, **219** (1960) 75.
[27] AMARAL L. A. N., BARABÁSI A. L. and STANLEY H. E., *Phys. Rev. Lett.*, **73** (1994) 62.